Beam characterisation studies of the 62 MeV proton therapy beamline at the Clatterbridge Cancer Centre

Jacinta Yap[a,b,*], Javier Resta-López[a,b], Andrzej Kacperek[c], Roland Schnuerer[a,b], Simon Jolly[d], Stewart Boogert[e], Carsten Welsch[a,b]

[a] *Cockcroft Institute, Warrington, WA44AD, United Kingdom*
[b] *University of Liverpool, Merseyside, L693BX, United Kingdom*
[c] *The Clatterbridge Cancer Centre NHS Foundation Trust, Wirral, CH63 4JY, United Kingdom*
[d] *University College London, University of London, London, WC1E 6BT, United Kingdom*
[e] *John Adams Institute at Royal Holloway, University of London, Egham, TW20 0EX, United Kingdom*

Abstract

The Clatterbridge Cancer Centre (CCC) in the United Kingdom is the world's first hospital proton beam therapy facility, providing treatment for ocular cancers since 1989. A 62 MeV beam of protons is produced by a Scanditronix cyclotron and transported through a passive delivery system. In addition to the long history of clinical use, the facility supports a wide programme of experimental work and as such, an accurate and reliable simulation model of the treatment beamline is highly valuable. However, as the facility has seen several changes to the accelerator and beamline over the years, a comprehensive study of the CCC beam dynamics is needed to firstly examine the beam optics. An extensive analysis was required to overcome facility related constraints to determine fundamental beamline parameters and define an optical lattice written with the Methodical Accelerator Design (MAD-X) and the particle tracking Beam Delivery Simulation (BDSIM) code. An optimised case is presented and simulated results of the optical functions, beam distribution, losses and the transverse rms beam sizes along the beamline are discussed. Corresponding optical and beam information was used in TOPAS to simulate transverse beam profiles and compared to EBT3 film

*Corresponding author.
Email address: jacinta.yap@liverpool.ac.uk (Jacinta Yap)

measurements. We provide an overview of the magnetic components, beam transport, cyclotron, beam and treatment related parameters necessary for the development of a present day optical model of the facility. This work represents the first comprehensive study of the CCC facility to date, as a basis to determine input beam parameters to accurately simulate and completely characterise the beamline.

Keywords: Proton therapy, passive delivery, monte carlo, simulation, modelling, beam optics

1. Introduction

Significant advancements in accelerator technology and growing experience with the use of ion beams for medical applications has supported the recent emergence of charged particle therapy facilities worldwide [1]. The benefit over conventional X-ray radiation therapy stems from the advantage of delivering a beam with a finite range. Protons undergo interactions due to their mass and charge, continually slowing down before they come to a complete stop, resulting in a culmination of energy deposition: the 'Bragg Peak'. After this point there is negligible transfer of energy, allowing the beam to be manipulated and delivered to targeted sites for the purposes of treatment.

The Clatterbridge Cancer Centre is one of a few dedicated ocular proton therapy clinics in the world [2], operating a fixed horizontal beamline which delivers protons at 60 MeV at isocentre using a double scattering system. This produces a conformal beam with a range of 31 mm and a sharp fall-off (0.9 mm), enabling the targeted and precise delivery of uniform dose to tumour volumes. High rates of local tumour control, ocular retention and preservation of visual acuity have been achieved and patients with ocular melanoma have been successfully treated for almost 30 years [3, 4]. Since the first set of eye patients in 1989, there are now over 70 proton therapy facilities in operation worldwide. The majority operate at higher energies (i.e. >160 MeV), utilising various delivery methods and arrangements of cyclotrons, synchrotrons or synchrocyclotrons for acceleration and beamlines and gantries for delivery [5].

Although there is a demand for higher energy beams which can treat a greater range of cancers with conformal techniques and penetrate through to deeper seated tumours, there still remains a need for dedicated ocular

treatment beams [3, 6]. Uveal melanomas have the highest incidence rate for adult ocular tumours and although treatment using other methods are possible, proton beam therapy is considered the gold standard treatment modality for these cases [7]. Clinical protocols have been well developed by early facilities such as Clatterbridge; although these may vary across centres, the ongoing experience and practised delivery of exploiting the sharpness of the distal edge enables a large volume of patients to be treated effectively.

1.1. Facility and treatment considerations

High energy, multi-room facilities require an energy selection system (ESS), including degraders in the gantry or further upstream to decrease proton energies to levels applicable for eye treatments. This introduces additional considerations to the transport and design of the beamline and also results in several differences to the beam quality and properties. Extensive details can be found in literature [5, 8, 9, 10, 11] however for the context of ocular treatments, we mention some key physical characteristics. Facilities which operate at close to the maximum machine energy are able to generate a fixed, passively scattered beam with minimal energy or range straggling effects. This makes it possible to produce a beam with a steep Bragg Peak fall-off whereas higher energy beams require the presence of a degrader which also decreases transmission. Hence, consistent beam penumbrae and distal-off characteristics can be achieved regardless of the treatment prescription; these parameters remain until the beam is modified for patient specific conditions. Moreover, there is no time lost waiting on the ESS to switch between energies and short treatment times are particularly important for the patient experience. Quality assurance procedures are performed to maintain typical and local treatment beam requirements. The required beam parameters for general ocular treaments are discussed in detail in [2, 6]. A summary of these as also applicable for CCC, is provided below in Table 1.

Table 1: General treatment beam parameters [2].

Parameter	Value
Dose rate	8-30 Gy/min
Set-up time	10-15 mins
Treatment time	30 secs
Verification precision	± 0.2 mm
Field uniformity	<1%
Field diameter	<34 mm
Penetration depth	4-29.3 mm
Fall-off	0.9 mm (90 - 10%)
Penumbrae	1.1 mm (80 - 20%)

Modern facilities constructed by major turnkey vendors often feature the same or related designs, systems and commissioning procedures to enable higher consistency with day to day operation. This includes acceptance and commissioning tests to study, verify and characterise the beam. Minimal requirements and standards of performance must be met before initial or regular clinical operation; these must also be maintained across the lifetime of the equipment. As each facility or individual machine may be different, these procedures differ across locations, especially those built much earlier. The extent of characterisation and study may be limited as they are most often unique facilities.

Consequently, there is no pre-existing optics beamline model for CCC; a feasibility study for energy upgrades [12, 13, 14] and beam emittance and transport work was done in the past [15, 16]. In the latter, results are inconclusive and there has been little attempt since to combine all findings and understanding of the beam dynamics for practical use. Any relevant historical information documented originates from the period of time prior to and surrounding the beamline conversion, thus only pertains to it's operation for neutron therapy. Despite this, the beam requirements for treatment fall within defined ranges (Table 1). In practice the operation of the accelerator and beamline remain consistent as performance is maintained with routine checks.

Nevertheless, it is difficult to accurately model the treatment beam without knowing the characteristics and distribution of the beam generated be-

tween the delivery system and the exit of the cyclotron. As there is an absence of functioning diagnostic systems upstream of the treatment room, a practical approach is to examine the beam dynamics. This enables the beam to be characterised across the entire beamline. In particular, to determine properties of the beam at the start of the treatment line as pertinent for input parameters for simulation models.

Therefore this work is a retrospective study of sorts, to accurately model an established proton therapy facility given the arrangement of the beamline, components, cyclotron settings and magnetic parameters as they currently stand. Several codes were used to develop an optical lattice of the facility and generate a beam distribution which is compared with film measurements. CCC has a long history of clinical treatment, supporting a wide and diverse scope of experimental work and still remains as one of the pioneering facilities for proton therapy. As such, this study serves as a basis for accurate simulation modelling, beamline upgrades, optimisation, testing and integration of diagnostics, with possible application for similar facilities.

2. Materials and Methods

2.1. Clatterbridge Cancer Centre

The Douglas Cyclotron and beamline was built and commissioned in 1984 initially for fast neutron therapy trials [3] before becoming a proton therapy service. Further construction was required to accommodate a supplementary treatment room [17] and parts of the early beamline are still contained within the cyclotron bunker. These however are no longer in use, along with several other components displayed in Fig. 1. The flip screens (FS), stray beam detectors (SBD) and beam profile monitors (BPM) which are shown in the plan but have been removed.

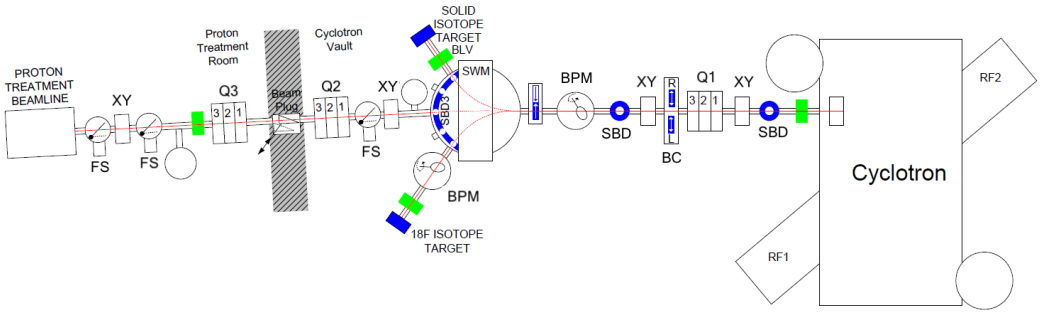

Figure 1: Original layout of the complete CCC beamline. Within the vault, the cyclotron produces the proton beam (red line) which passes through the transport line comprising various components and magnets, to the treatment room area. Notable beamline elements; quadrupoles (Q), dipoles (X), switching magnet (SWM) and beam collimator (BC), full listing can be found on [18].

The Scanditronix MC-60 PF isochronous cyclotron generates a 62 MeV beam of protons transported through nine quadrupoles arranged into three triplets, a switching magnet and collimators before leaving the bunker and onto the passive delivery system in the treatment room (Fig. 3a). The treatment beamline was designed to deliver a clinically useful beam, employing a double scattering system to produce a uniform beam. Range shifting or modulation devices can be inserted just downstream of the scatterers, this location was found to minimise penumbra and subsequent energy losses [3, 17, 19]. As illustrated in Fig. 3b, this includes two tungsten scattering foils (A) with a brass stopper on the second foil, range modulator and wheel (B & C), several collimators (E), two dose monitors (F), tungsten cross-wires (G) and a final brass nozzle and collimator (H). Functional parameters of the cyclotron generated proton beam are listed in Table 2.

Table 2: CCC beam parameters.

Parameter	**Value**
Ion type	p^+
Nominal kinetic energy	62 MeV
Beam current (maximum)	1-30 (50) nA
Energy spread	0.1%

Figure 2: Scanditronix MC-60PF Cyclotron and first quadrupole triplet.

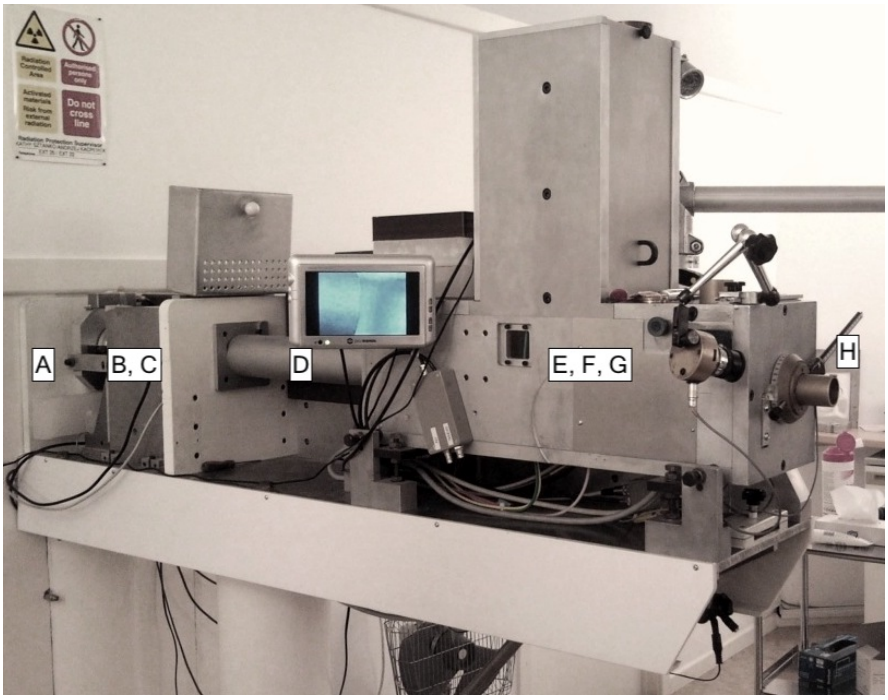

(a)

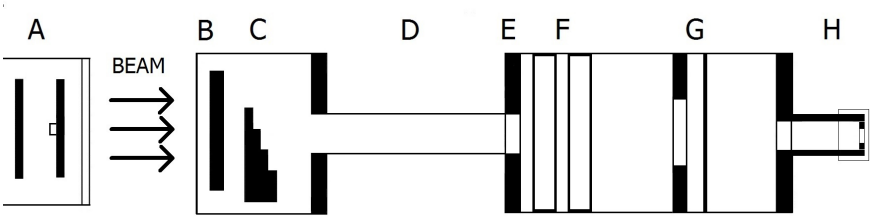

(b)

Figure 3: a) The treatment room beamline; the proton beam originates from the accelerator bunker behind the wall, exiting vacuum after it passes through two scattering foils (A) and a Kapton window. b) Schematic of the delivery system and beam shaping components. Cross-wires (G) and ionisation chambers (F) upstream of the end nozzle (H) are used to routinely monitor the uniformity and performance of the beam.

2.2. Beamline elements

An accurate description of the beamline components is necessary and specifically, the parameters of the magnetic elements which comprise the optical lattice must be defined for beam simulations.

Geometrical measurements were taken across the entire beamline (Table 3) for all relevant components in both the demarcated bunker and treatment room areas. As the beamline is permanently fixed in place and the beam pipe passes through a concrete wall, measurements were also checked against original floor plans [18]. The outer diameter of all the beam pipes were not uniform and it is unclear if this is due to changes in the thickness of the pipe walls or if the inner dimensions also change. The minimum inner radii was surveyed to be 30 mm and this was assumed for the simulations.

It is mentioned in [16] that the first BC after Q1 (Fig. 1) is an actuated collimator. Presumably, it was installed to remove the beam halo or tails [20] which skew the shape of the beam asymmetrically, causing the larger horizontal emittance. The collimator minimises the beam spread and dispersion of the beam envelope specifically as it enters the switching dipole. Here the magnetic field results in separation of particles, further horizontal beam growth and a magnified tail downstream; BC mitigates radiation losses and improves the beam quality for treatment.

2.3. Magnets

For the magnets, defining the physical dimensions was more problematic as the quadrupoles were grouped into triplets with their individual yokes and coils obscured from view (Fig. 4a). Schematics were only available from initial neutron therapy line designs and it is not feasible to move or disassemble any elements. Therefore, dimensions were inferred by checks against original manufacturer drawings and the geometry for the second and third quadrupole were extrapolated from Q1. The switching magnet (Fig. 4b) was originally used to divert the beam to other beamlines for neutron production. The SWM has a deflection angle of 5.5° which has only slight influence on the beam optics.

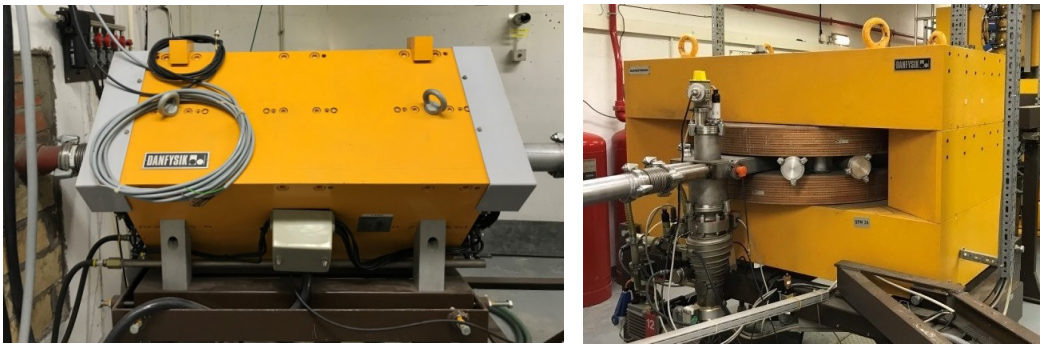

(a) (b)

Figure 4: Close up of the second quadrupole triplet, Q2 (a) and switching magnet, SWM (b).

Magnetic fringe fields can also be modelled in the simulation code and this relates to the difference between the physical and effective lengths. For simplicity, fringe field effects were discounted by equating the total effective lengths to physical lengths, as displayed in Table 3. A lack of information and accessibility meant that drift distances (exterior to the iron core length) between the quadrupoles were estimated. Different lengths were simulated and smaller gaps were observed to cause blow ups in the optics further downstream, therefore a drift gap of 0.13 m was designated for all the triplets. Exterior magnet dimensions were known from physical measurements, this total length (of a triplet) accommodates multiple drift spaces and effective lengths as compensated by each quadrupole equally (Fig. 5). In the event that more precise information is determined in the future, the optical lattice can be matched by modifying the relevant parameters.

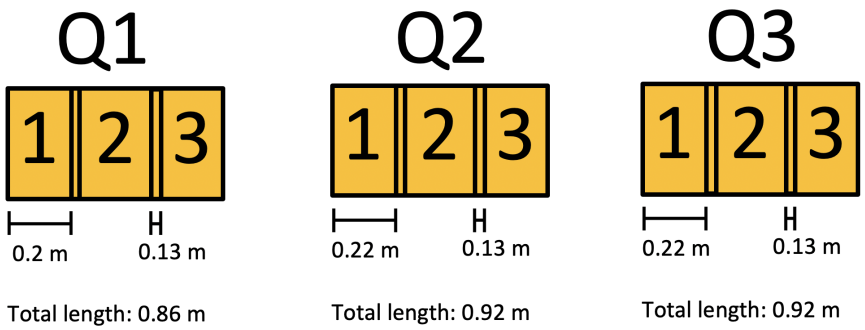

Figure 5: Sketch of the quadrupole triplets. Determined dimensions of the effective lengths and drift spaces are shown.

2.3.1. Nominal quadrupole field gradient

It is also important to describe each quadrupole in terms of their magnetic strength or field gradient. This presented complications, requiring that the limited information provided by the manufacturer and from the control system be converted into relevant quantities. Each quadrupole triplet had recommended operational parameters stated for each magnet and these were scaled and optimised. As the field coverage was approximated to the effective length of each quadrupole, a linear correlation was assumed to calculate the normalised quadrupole gradients K_I. This is based on the listed field gradients and nominal current for each quadrupole, multiplied with the programmed currents. This provides an estimate of each field gradient: the generated field gradient $G = I \times K_I$, where I is the supplied current. The normal quadrupole strength is determined by taking this field gradient over the beam rigidity and corresponding nominal values are also listed in Table 3. The treatment line is indicated to begin 2.59 m downstream of Q3. Combined with the beam transport line, the entire beamline has a length totalling 17.92 m from the exit of the cyclotron to the treatment nozzle.

Table 3: Nominal parameters and lengths of beamline elements

Element	**Physical Length [m]**	**Effective Length [m]**	**Normal Quadrupole Strength [m^{-2}]**
Q11	-	0.20	-11.93
Q12	-	0.20	7.35
Q13	0.86	0.20	-6.40
Q21	-	0.22	4.14
Q22	-	0.22	1.21
Q33	0.92	0.22	-4.14
Q31	-	0.22	5.89
Q32	-	0.22	-10.92
Q33	0.92	0.22	5.89
SWM	1.13	0.85	-
Transport line	16.15	-	-
Treatment line	1.77	-	-
Cyclotron to Nozzle	17.92	-	-

2.4. Simulation modelling

Two simulation codes were used to model the optical lattice, Methodical Accelerator Design (MAD-X) [21] and Beam Delivery Simulation (BDSIM) [22] (Section 2.4.2). In order to generate an optical lattice of the facility, knowledge of fundamental beam properties such as the Twiss parameters and the emittance at the source point or exit of the cyclotron, are necessary to define the input beam source for simulation codes. This information was either unknown, inconsistently documented or irretrievable. Extensive review of documentation was necessary to locate any relevant information from studies performed in the past [12, 15]. The more recent work in [15], reports emittance and Twiss parameters determined by quadrupole variation scans (QVS) at the entrance of the first quadrupole. These are listed in Table 4 and are assumed to be equivalent to the extraction point of the cyclotron. This study encountered several uncertainties and these parameters do not agree with historically documented measurements [12] (i.e. ϵ_x = 4.2, 3π, 2 & ϵ_y = 6.6, 3π, 1.5 mm mrad). However, it is recognised that these values would differ given the changes to the cyclotron and facility over time, as detailed in [17]. As these are the most recently reported values, they were retained as input parameters for these beamline simulations.

Table 4: Reported Twiss parameters, dispersion and rms (1-σ) emittances at the cyclotron exit and nominal input parameters for this study [16].

Parameter	**Horizontal (i=x)**	**Vertical (i=y)**
Twiss Alpha (α_i)	0.8600	0.2685
Twiss Beta (β_i)	1.9897	1.0629
Dispersion (D_i)	0	0
Transverse Emittance (ϵ_i)	5 mm mrad	1 mm mrad

2.4.1. Optical lattice optimisation

The CCC beamline was defined in MAD-X using the optical lattice of the transport line combined with nominal parameters (Tables 2, 3 and 4). By providing a description of the input beam and a sequence of magnetic elements, it is possible to obtain the Twiss functions which describe the beam envelope throughout the beamline. The tool performs beam dynamic calculations to determine the beam ellipse at a point which can also be transported to various locations. As a result, the beam phase space can be determined

at any arbitrary position which allows the flexibility to match components and parameters to generate outputs as needed.

As mentioned in Section 2.3.1, the normal quadrupole coefficients listed in Table 3 are approximated. Therefore a process of optimisation was necessary to obtain minimal beam sizes and higher transmission. This was performed by applying a range of factors to further scale the strengths of each quadrupole triplet and resulting effects on the optical functions, transmission and calculated beam sizes along the transport line were assessed. As these are primarily dependent on the extent and evolution of the beam envelope, the Twiss functions were optimised to reduce erratic or large fluctuations such that outputs within beamline constraints could be achieved, these are further discussed in sections 2.5 and 2.4.2. Q1, Q2 and Q3 were finally scaled by 0.3, 0.8, 0.8 respectively and the optimised set of simulated Twiss functions are shown in Fig. 6.

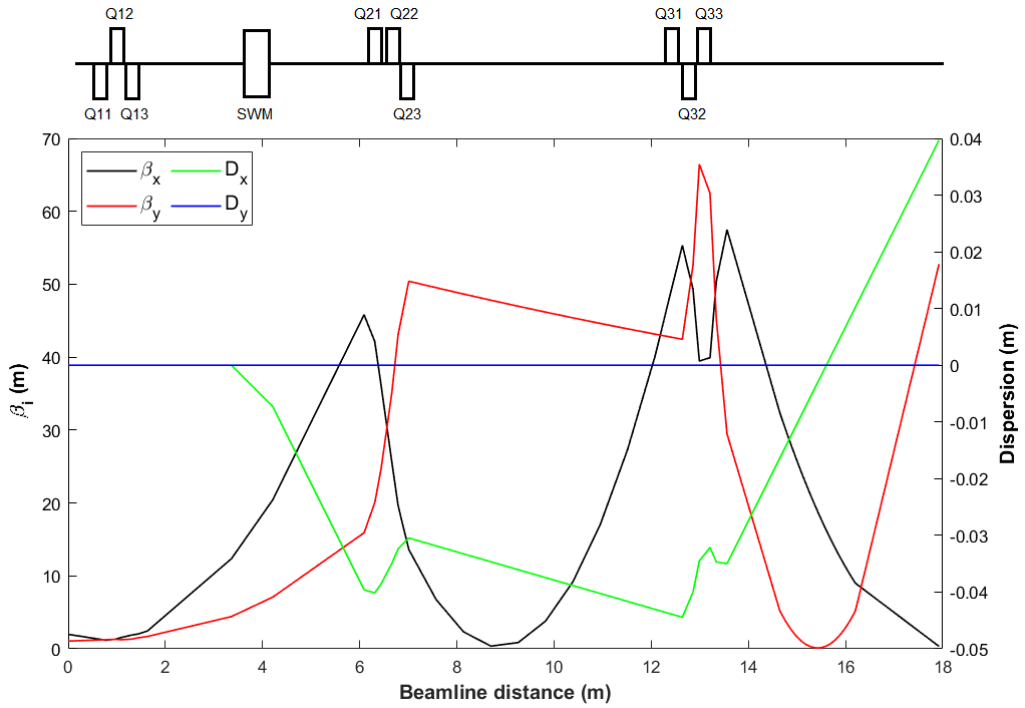

Figure 6: Twiss functions (Twiss beta β_x, β_y and dispersion D_x, D_y) for the nominal case, across the entire beamline starting from the cyclotron exit (0 m) to the nozzle (17.92 m). The magnetic elements are displayed above the plot.

2.4.2. Beam distribution

The optical lattice was also simulated in BDSIM, to look at other aspects of the beamline as useful for beam characterisation and for future inclusion into a complete end-to-end model. The code utilises the Geant4 toolkit [23, 24, 25] to simulate the beam distribution, transport, particle losses, interactions and also has the capability of building detailed 3D geometries. For the scope of this study and specific applicability for the facility, BDSIM was used to visualise the beam distribution (Fig. 7), benchmark the MAD-X beta functions (Fig. 8) and for an analysis of the beam transmission (Fig. 11).

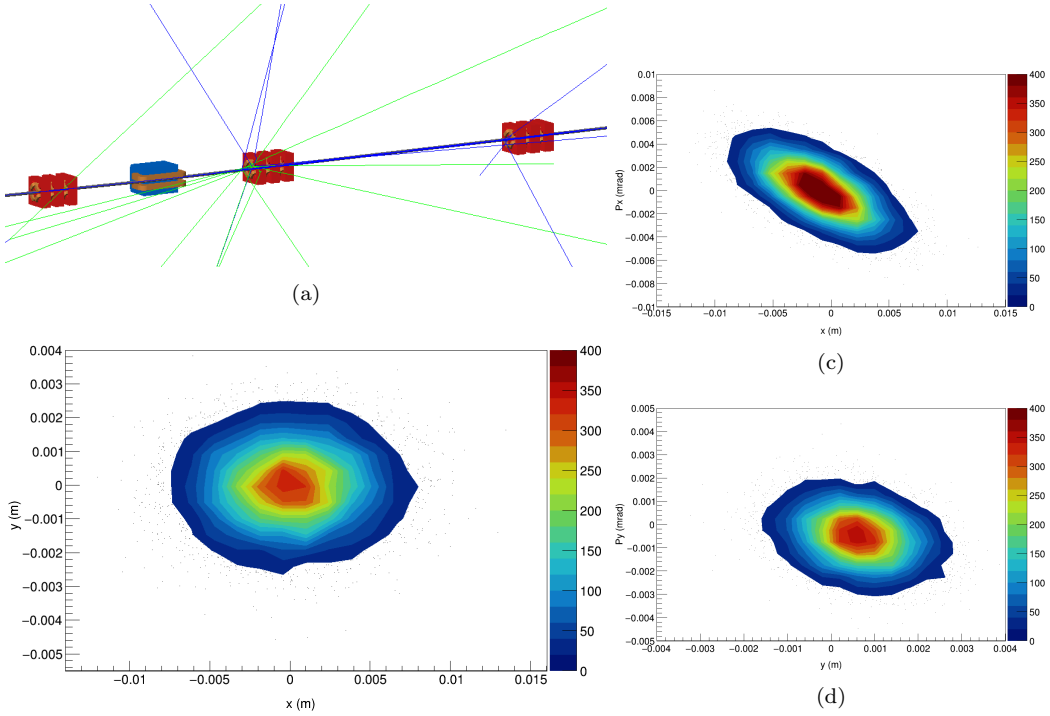

Figure 7: a) CCC beamline modelled in BDSIM displaying trajectories of protons (blue) and secondary particles (green). Beam distribution at the exit of the cyclotron in the transverse plane (b) and phase space ellipses in the x (c) and y direction (d).

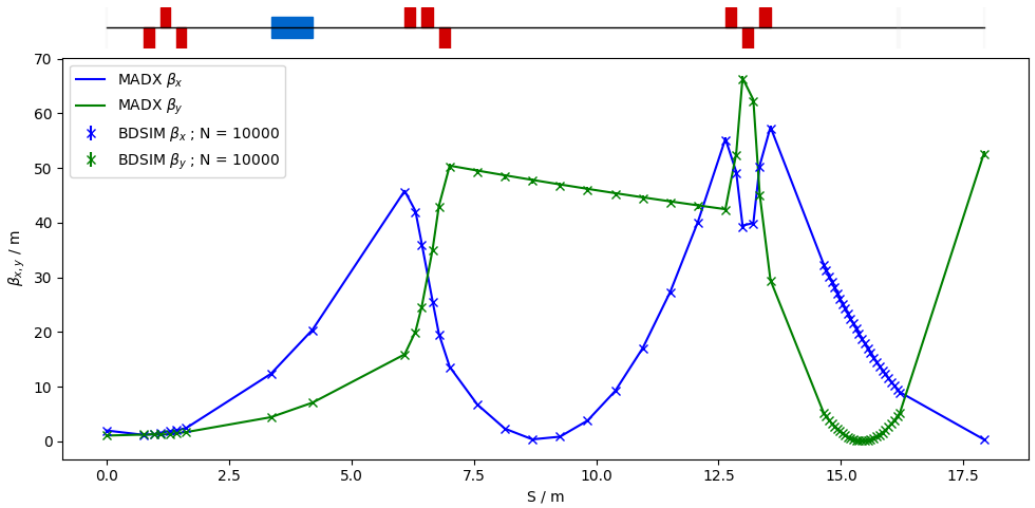

Figure 8: Comparison of Beta function plots between MAD-X (solid line) and BDSIM (markers) in the x and y direction for 10,000 primaries.

2.5. Transverse beam size

As necessary for this study, these optimised distributions and Twiss functions were further examined for the extent of their physical implications: specifically to determine rms transverse beam sizes. The divergence and size of the beam is essential when considering geometrical constraints of equipment (i.e. beam pipe, collimators) as well as for integration of any instrumentation into the beamline, either in the transport line or further downstream. Therefore beam sizes at several important locations were evaluated using the following equation:

$$\sigma_i = \sqrt{\beta_i \epsilon_i + {D_i}^2 \left(\frac{\triangle p}{p}\right)^2} \tag{1}$$

where σ_i is the transverse rms 1-sigma beam size and i denotes the horizontal (x) or vertical (y) direction. This is determined by the Twiss beta β_i, transverse emittance ϵ_i, dispersion D_i and the square of the relative rms momentum spread $\Delta p/p$. Furthermore, a correction was required to account for the spread in kinetic energy and momentum:

$$\frac{\triangle p}{p} = \frac{\gamma}{\gamma + 1} \frac{\triangle E_k}{E_k} \simeq 0.5160 \cdot \frac{\triangle E_k}{E_k} \tag{2}$$

In this case, $\Delta E_k/E_k$ is the kinetic energy spread of the Scanditronix cyclotron (Table 2) and γ is the Lorentz factor which is determined by:

$$\gamma = \frac{E}{m_o c^2} = 1.066 \tag{3}$$

The calculated transverse rms sigma values are plotted against distances along the beamline and displayed in Fig. 9. To examine the reliability of the nominal emittance (red), two other emittance values were also used to calculate beam sizes as reported in [12] (blue) and by the manufacturer (green). A diagram of the magnets has been overlaid for approximate comparison.

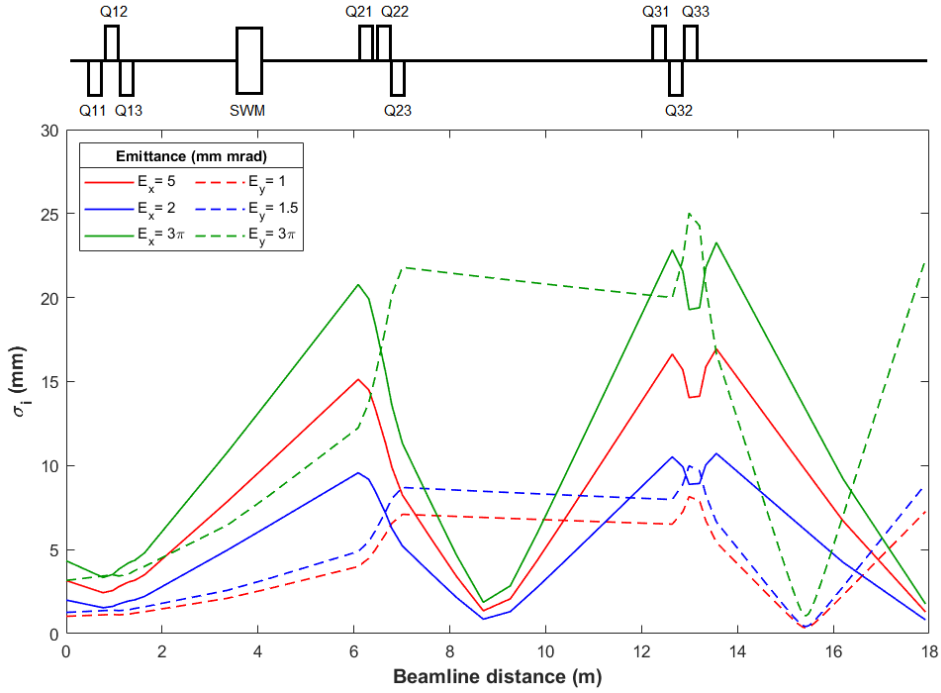

Figure 9: RMS beam sigma values for x (solid line) and y (dashed line) across the entire beamline for different emittances. The nominal emittance (red line) is utilised for this study.

2.6. Beam profile measurements

The start of the treatment line is indicated to begin at 16.15 m (Table 3). In accordance, this is also assigned as the beam source plane location for the simulations in TOPAS. The significance of this location is also associated

with the close proximity to P1-P4, where measurements performed here may have additional uses secondary to the beam optics, by providing a direct determination of the beam profile. However, the closest accessible location to non-destructively measure the beam is 38 cm downstream of this point, where the beam exits the vacuum sealed scattering pipe (Fig. 3b) and enters the treatment room. As such, EBT3 Gafchromic^{TM} film [26] was attached to the downstream face of the Kapton window and irradiated to obtain relevant information to resolve the beam profile.

The use of EBT3 film in radiation therapy is well established, typically for machine quality assurance and as a visual check of beam characteristics. EBT3 is also commonly used to determine beam performance and quality in proton therapy. Its high spatial resolution and low energy dependence enables measurements of relative dose profiles as dose maps in the transverse plane [27]. Following exposure to radiation, the beam and dose distribution can be obtained by evaluating the range of pixel intensities across the film as it darkens and self develops. A close up of the Kapton window attached to the end of the scattering tube, affixed film and obtained beam spot is shown in Fig. 10.

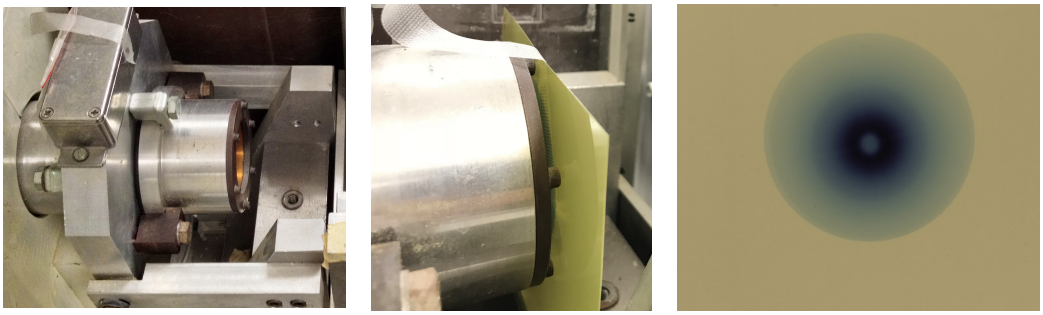

(a) (b) (c)

Figure 10: a) Scattering tube protruding from the wall separating the cyclotron bunker. The beam exits the Kapton window (orange in appearance) and enters into the treatment room. b) Film setup. c) Beam spot on EBT3 film after irradiation and self development.

Moreover, it is noted that at the location of the film, the beam has passed through several components (two tungsten scattering foils and a brass beam stopper, Fig. 3b) which alter the shape and spread of the beam. This can be seen in Fig. 10c by the distinctive void in the central area of the beam spot, as intended by the delivery system design [19, 17]. Primarily due to the presence of the brass stopper, the proton fluence here is substantially reduced

such that the beam distribution will be flat and uniform at isocentre (70 mm after the end of the treatment nozzle). As the beam here has a modified shape and distribution, the optics calculations alone are insufficient to determine the corresponding size of the beam. As such, particle tracking simulations are necessary to obtain the beam distribution after it has traversed the scattering foils and beam stopper.

Simulations were performed using a model of the delivery system [28] developed with TOPAS (version 3.2.p1) [29], a code for proton therapy extended from the Monte Carlo simulation toolkit, Geant4. Outcomes of this beam dynamics study contribute to efforts to verify and validate this and other related models of the Clatterbridge facility [30, 31]. The input particle source was positioned at the designated start point of the treatment beamline and defined given known beam quantities and parameters determined from the optical model (Tables 1, 4, 5). The simulated beam distributions after the Kapton window are compared to those obtained with EBT3 gafchromic film (Fig. 13).

3. Results

3.1. Optimised beam parameters

As discussed in section 2.4.1, nominal parameters were calculated for each quadrupole and their gradients were normalised and scaled to generate an optimised optical lattice. As the resultant physical size of the beam is the primary consideration for our case, parameters were modified to decrease the bounds of the optical functions and thus maximise the beam transmission. BDSIM was used to simulate realistic beam distributions along the beamline and the corresponding beam losses.

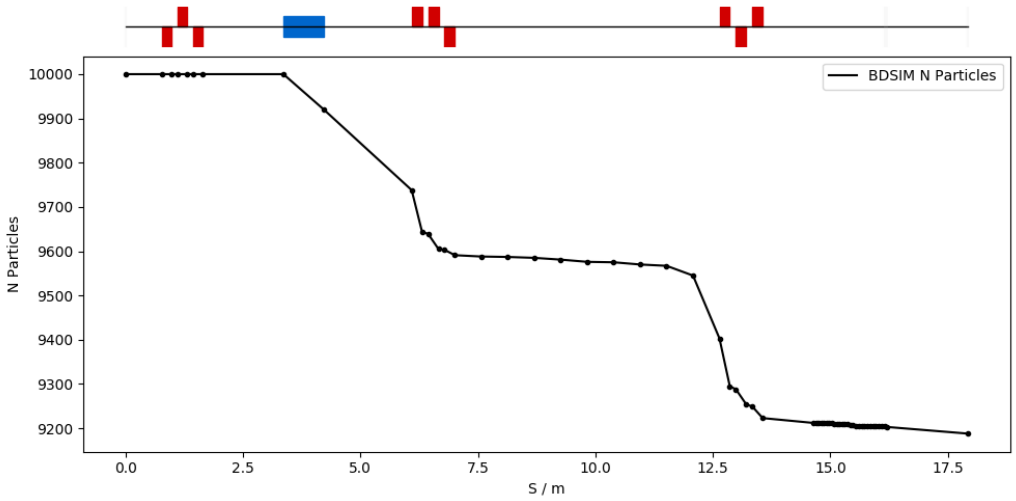

Figure 11: Particle losses across the beamline for 10,000 simulated primaries.

Further to scaling the normal quad strengths for each triplet, the resulting beam sizes were also examined as part of the optimisation process. Fig. 12 illustrates the wide range of possible beam sizes along the transport line as a result of changing the quadrupole parameters. Minimum or maximum σ_i are denoted by either a marker or line to indicate the boundaries at either extreme. Each marker or line type represents a set of either σ_x (red) or σ_y (blue) values which have been generated by applying a scaling factor to the nominal quadrupole strengths. For clarity, only the sets pertaining to the outer boundaries have been individually displayed. The remaining series of σ_i pairs are contained within the shaded region and the beam sizes determined for the nominal, optimised case are specified by the solid lines.

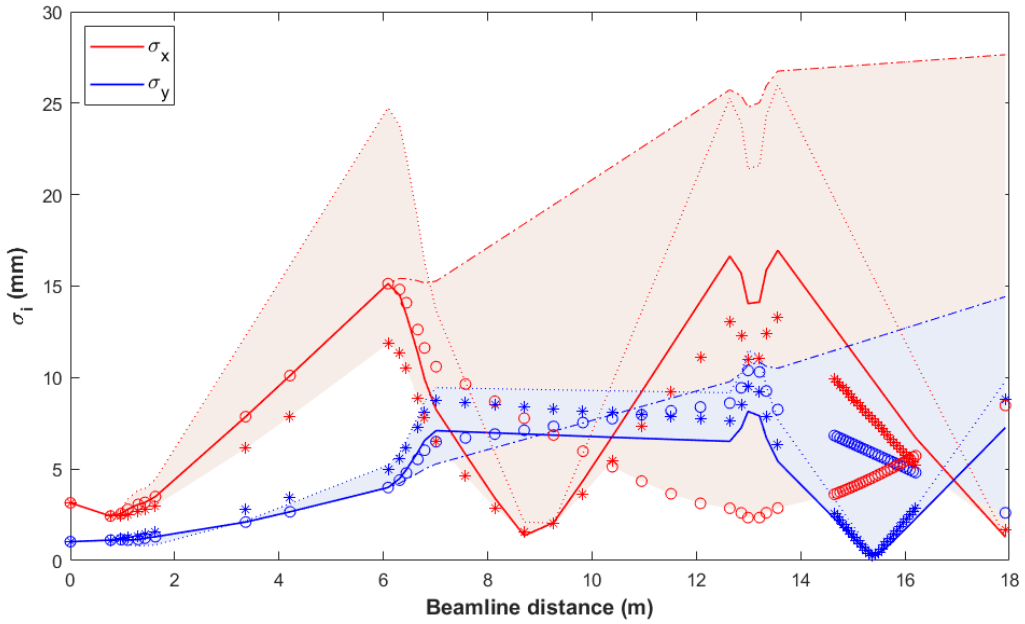

Figure 12: Ranges of possible transverse RMS beam sizes generated by varying the quadrupole gradients. The non-solid lines and markers correspond to the sets with maximum or minimum σ_x (red) and σ_y (blue) values. All other σ_i sets are contained within the shaded regions and the optimised case is indicated by the solid lines. As distances between 14.5-16.2 m are meaningful, smaller interpolation between these points are observed.

3.2. Beam sizes

Given our nominal and optimised case, the following rms beam sizes were determined and are listed in Table 5 with corresponding beta values.

Table 5: Optimised lattice beam sizes and betatron values.

Marker Location	**Distance** [m]	σ_x [mm]	σ_y [mm]	β_x [m]	β_y [m]
Cyclotron exit	0	3.15	1.03	1.99	1.06
After SWM	6.09	15.13	3.99	45.81	15.91
End of Q3	13.56	16.95	5.43	57.48	29.47
Diagnostics P1	14.65	12.73	2.29	32.42	5.25
Diagnostics P2	14.81	12.10	1.82	29.26	3.33
Diagnostics P3	14.97	11.46	1.36	26.27	1.85
Diagnostics P4	15.14	10.83	0.91	23.44	0.82
Treatment line start	16.15	6.89	2.14	9.52	4.59

3.3. Measured and simulated profiles

The film was irradiated, calibrated and evaluated using the red channel, given standard protocol (described in more detail in [32, 33]) to determine the transverse beam profile at the designated point (Fig. 10b). TOPAS was used to simulate a beam and obtain the dose deposition within defined material equivalent to EBT3, at the same position as the film. The dose distribution was scored in the x and y directions and plotted against position, representing corresponding beam profiles. These were compared to the transverse profiles obtained from film measurements and are presented in Fig. 13.

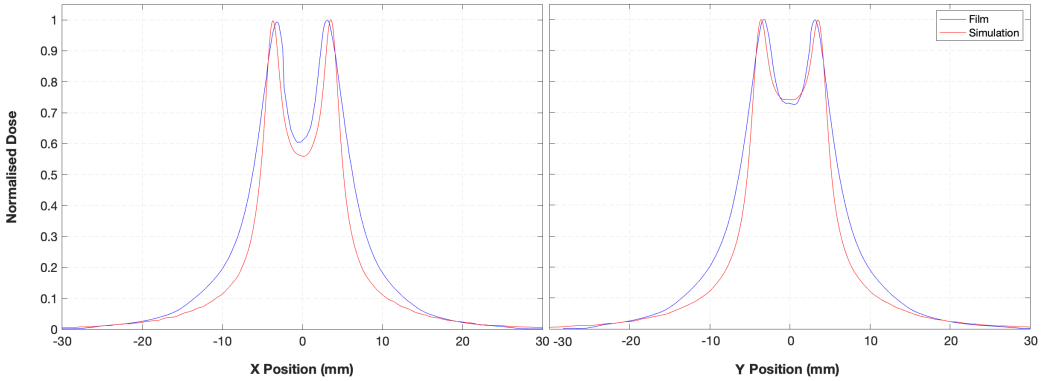

Figure 13: Transverse beam distributions in the X (left) and Y (right) direction. Film measurements (blue) are normalised to maximum doses obtained by conversion from optical density by standard protocol. Simulated profiles (red) have also been normalised to maximum doses for comparison.

In order to directly compare the two methods, plots were normalised to corresponding maximum values. The EBT3 film provides the geometrical beam distribution as a function of the dose, evaluated by converting the grey value of each pixel to a net optical density (OD). The OD is dependent on the extent of irradiation and thus each OD value results in a corresponding dose (Gy). The dose at this location is correlated to known quantities of radiation delivered to a (calibration) set of film irradiated at isocentre, determined by ion chamber measurements. A calibration curve obtained with this set enables conversion across the full dose range and takes into account corrections for minor deviations in grey values and saturation effects. The film was also found to have a slight tilt in the positive x direction and an adapted normalisation factor was applied to adjust for the non-uniformity. Furthermore, at this location the dose is a relative value (correlated to ion chamber further downstream) and the beam current would also be similarly approximated. However, as the beam current is proportional to dose and the deposition in film was directly simulated, results were also normalised to maximum dose and plotted according to position along the axis.

4. Discussion

4.1. Beam optimisation

This work provides an extensive overview of the beam optics of the Clatterbridge facility, as a means to model and characterise the beam for medical physics and research purposes. Several codes have been used to simulate the propagation and distribution of the beam, optimising parameters and the optical functions to assess the impact on physical beam properties in order to generate a representative, nominal model.

Starting with our developed Twiss functions (Fig. 6), we see the increase in dispersion in the negative direction (across the x plane) beginning around the switching magnet but it remains constant at 0 in the y plane as the magnetic field generated by the dipole bends the particles in the beam only across one plane. The switching magnet was initially responsible for diverting the beam to the different beamlines but now just deflects the beam slightly hence only has a small dispersive effect. The betatron functions β_i are dependent on the fields produced by the quadrupoles and describe the orientation and divergence of the beam. The beam envelopes converge following passage through the first and second quads, however the overall changes to the optical functions show a clear increase from initial beam parameters. Similarly,

in Fig. 9 we see the physical changes in the transverse beam sizes as largely dependent on the optical Twiss functions. These can be observed to similarly follow the distribution of these beta curves in Fig. 6.

We further modelled this in BDSIM, to visualise and determine the beam size at any given point throughout the beamline. As observed in Fig. 8, the code also models the optics functions consistent with MAD-X: both plots are observed to agree well. Furthermore, given these simulation conditions, we obtain a transmission of 92% from the exit of the cyclotron to the end of the treatment line (Fig. 11). As this is an optimised case, it suggests that minimum beam losses of 8% are expected with this optical lattice arrangement and assumed parameters. Large numbers of particles are lost after the SWM as the growth in dispersion here causes an increase in the beam σ_x. Significant losses occur where there is high dispersion, as seen at points of entry to Q2 and Q3. Once the beamline and quadrupoles have been characterised, it could be possible to improve the actual transmission efficiency. Low losses across the transport line are ideal as once the beam enters the treatment line, transmission dramatically reduces to a few percent. This is caused by beam traversal through multiple components in the delivery system or gantry to shape and correct the beam as dependent on the needs for treatment. As purposed, the scattering system and shaping components collimate and modify the distribution to such an extent that the beam delivered for treatment will remain consistently within specified constraints. Consequently, at this point the uncertainties associated with this model and its representation of the actual treatment beam and quality achieved at isocentre has a limited and unforeseen impact. Nonetheless, what is most applicable in our study is the determined distribution and size of the beam, as a basis for beam parameters at the start of this treatment line.

4.2. Beam Sizes

The lattice is designed such that the beam is delivered with qualities to fulfil its operational purpose. For operation at CCC, this mostly involves altering the magnetic fields to transport a small and flat beam (uniform transverse distribution) through the treatment nozzle. A smaller beam is desired to maximise transmission, to avoid losses from interactions with the beam pipe wall or parts of components which may obstruct the beam path. This was achieved by the geometrical arrangements of quadrupoles into triplets and by changing the quadrupole field strengths or polarities, resulting in stronger or weaker focussing in one or the opposite plane.

In reality, this generates a beam which should be less than the minimum 60 mm pipe diameter which can traverse the vacuum pipe at the beginning of the treatment beamline (>16.15 m) with sufficient transmission. Ideally at this point the beam size should be small enough as the pipe contains a first collimator of diameter 6 mm, which was considered when optimising the lattice. At this stage the beam sigma has doubled in comparison to the start of the transport line; additional beam sizes and corresponding betatron values at significant locations and potential positions for diagnostics (P1-P4) are also listed in Table 5. As these values are contingent on the reliability of the information and parameters used in the simulation, experimental measurements are necessary to benchmark this lattice. However, this cannot be done non-destructively as the quadrupole specifications cannot physically be checked and thus have been approximated to their best degree. As such, our approach was to modify the normal quadrupole gradients to match actuality.

Consquently, Fig. 12 demonstrates that varying the magnet settings results in a large range of beam sizes. This is most significant at >12 m, where knowledge of the beam parameters is most important. Therefore, experimental measurements can verify the precision of this model, which can be benchmarked by determining the emittance or transverse beam profiles under standard or defined accelerator settings. This is straightforward for modern facilities which already have diagnostics devices [34, 35] installed in their transport lines; for this case however, a system would need to be designed and integrated into CCC. In terms of both the physical design and optics, locations P1-P4 were identified as the most ideal sites for system integration for experimental measurements. These can be done using several different methods, most suitably either; pepper pot, quadrupole variation scans (QVS) or multiple profile measurements [36, 37, 38]. Given the nature of the facility and beam, a combination of the latter two with a scanning fiber system [39] is anticipated. It is aimed that measurements with this system using multiple methods will yield Twiss parameters, emittances and also allow simultaneous characterisation of the quadrupoles. However, as the integration of any diagnostics devices interferes with clinical operation and requires dissembling of the beam pipe and components, a measurement of the transverse beam profile at the beginning of the treatment line was performed with EBT3 film as a baseline check.

4.3. Treatment line beam profiles

Comparing the film with the simulated profiles (Fig. 13), we see similar distributions however a larger penumbra is observed for both cases, with slight deviation in the central aperture regions (5% and 2% differences for x and y, respectively). This is partly attributed to the process of conversion from net OD, where higher uncertainties were associated with smaller dose or net OD values. The exponential nature of the calibration curve mean that at this lower end, marginal variations in ODs may result in augmented doses. For the profile in x, the film exceeds the simulated dose of up to approximately 30% and 20% in y. Experimental uncertainties also contribute to these variances as the film measurements are dependent on the beam quality on the day. Furthermore, additional simulation studies showed that the beam is likely to diverge more if the beam size was originally underestimated: a smaller input beam will propagate and end up with a greater lateral spread in comparison to a bigger input beam, at the same position. However, given the larger emittance in x, these lower dose tails may also originate from differences in the scattering system geometry or additional scatter and interactions which were not sufficiently modelled.

Good agreement between the simulation and experimental profiles is observed at the highest regions of dose. While testing the model with different input beam parameters, it was also noted that the beam distribution remained mostly unchanged except for the extent and elevation of the centre dip. However, as all factors influence the beam shape, it was unclear which parameter (beam size, angular spread etc.) had the most significant effect. The differences between the two graphs are also evident of this, as the brass stopper has the same radius and extrusion in either (x or y) direction but we see less attenuation in y. Both the beam size and emittance are smaller in y, indicating less spread, a slightly smaller beam width and less reduction to the apex. The better congruence in y suggests that the optical parameters are more realistically modelled than for x.

Given these considerations, measurements with a direct method such as a silicon detector or beam profile monitor could provide a better indication of the absolute distributions in the transverse plane. Varying the input emittance could also result in better consistency between the plots. Nonetheless, the agreement between these distributions suggests the applicability of the optical study derived parameters to simulate a physically similar beam. It is clear that at this point the beam divergence and distribution are influenced by the input beam parameters. These results yield similarities to simula-

tions and improvements are anticipated with further emittance and profile measurements.

5. Conclusions

Following the change from a neutron to proton therapy service, this study is the first comprehensive overview of the beam dynamics of the Clatterbridge Cancer Centre proton therapy beamline. Treatment requirements and present day conditions of the facility and transport line provided constraints to define a model of the beamline simulated in both MAD-X and BDSIM. All existing beamline information was reviewed and the quadrupole parametrisation, simulated optical functions, rms transverse beam sizes and transmission efficiency was investigated. The developed optical lattice can be modified to match abitrary parameters but given discussed limitations, an optimised case was studied. Input beam parameters derived from optics calculations were used in TOPAS to generate beam profiles and these simulated beam distributions were compared with EBT3 Gafchromic film measurements as a baseline check. Similarities suggest the applicability of parameters determined from the developed optical lattice where the model can be further verified with experimental measurements.

This work aims to benefit the facility by providing a better understanding of the beam produced by the cyclotron and transported through the present arrangement of magnetic components as ultimately delivered for patient treatment. We present an extensive analysis of the linear beam optics of the CCC transport line as necessary for upgrades, integration of instrumentation and most significantly, to precisely model and completely characterise the beamline.

Acknowledgements

We would like to express gratitude to our colleagues for many helpful discussions which supported this study. Thank you Tomasz Cybulski, Hao Zhang, Hywel Owen, Alexandra Alexandrova, Chris Edmonds, Volodymyr Rodin, Lina Hoummi & Ewa Oponowicz. Further thanks to Matthieu Hentz, the original developer of the CCC Geant4 model. The authors also appreciate the provision of beamline information and technical assistance from Brian Marsland, Ian Taylor and Oleg Karamyshev. This research was funded by the European Union FP7 grant agreement 215080, Horizon 2020 research and

innovation programme: Marie Skłodowska-Curie grant agreement no. 675265 - Optimization of Medical Accelerators (OMA) project and the Cockcroft Institute core grant STGA00076-01.

References

[1] H. Owen, A. Lomax, S. Jolly, Current and future accelerator technologies for charged particle therapy, Nuclear Instruments and Methods in Physics Research, Section A: Accelerators, Spectrometers, Detectors and Associated Equipment 809 (2016) 96–104.

[2] A. Kacperek, Ocular Proton Therapy Centers, in: Ion Beam Therapy: Fundamentals, Technology, Clinical Applications, 2012, pp. 149–177.

[3] A. Kacperek, Protontherapy of eye tumours in the UK: A review of treatment at Clatterbridge, Applied Radiation and Isotopes 67 (2009) 378–386.

[4] B. Damato, A. Kacperek, D. Errington, H. Heimann, Proton beam radiotherapy of uveal melanoma, Saudi Journal of Ophthalmology 27 (2013) 151–157.

[5] H. Owen, R. MacKay, K. Peach, S. Smith, Hadron accelerators for radiotherapy, Contemporary Physics 55 (2014) 55–74.

[6] J. Hrbacek, K. K. Mishra, A. Kacperek, R. Dendale, C. Nauraye, M. Auger, J. Herault, I. K. Daftari, A. V. Trofimov, H. A. Shih, Y. L. E. Chen, A. Denker, J. Heufelder, T. Horwacik, J. Swakoń, C. Hoehr, C. Duzenli, A. Pica, F. Goudjil, A. Mazal, J. Thariat, D. C. Weber, Practice Patterns Analysis of Ocular Proton Therapy Centers: The International OPTIC Survey, International Journal of Radiation Oncology Biology Physics 95 (2016) 336–343.

[7] K. K. Mishra, I. K. Daftari, Proton therapy for the management of uveal melanoma and other ocular tumors, Chinese Clinical Oncology 5 (2016) 1–7.

[8] H. Paganetti, Proton Beam Therapy, volume 20115763, CRC Press, Boca Raton, Florida, USA, 2012.

[9] W. Wieszczycka, W. H. Scharf, PROTONTHERAPY ACCELERATORS, 2001.

[10] M. Schippers, Beam Delivery Systems for Particle Therapy: Current Status and Recent Developments, Reviews of Accelerator Science and Technology 2 (2009) 179–200.

[11] X. H. Zeng, J. X. Zheng, Y. T. Song, F. Jiang, M. Li, J. S. Zhang, W. Q. Zhang, L. Zhu, Beam optics study for energy selection system of SC200 superconducting proton cyclotron, Nuclear Science and Techniques 29 (2018) 1–8.

[12] J. A. Clarke, D. M. Dykes, C. W. Horrabin, H. L. Owen, M. W. Poole, S. L. Smith, V. P. Suller, A. Kacperek, B. Marsland, An Updated Assessment of a Medical Cyclotron As an Injector for an Energy Upgrade, in: Proceedings of EPAC1998, Stockholm, 1998, pp. 630–632.

[13] U. Amaldi, P. Berra, K. Crandall, D. Toet, M. Weiss, R. Zennaro, E. Rosso, B. Szeless, M. Vretenar, C. Cicardi, C. De Martinis, D. Giove, D. Davino, M. R. Masullo, V. Vaccaro, LIBO - A linac-booster for protontherapy: Construction and tests of a prototype, Nuclear Instruments and Methods in Physics Research, Section A: Accelerators, Spectrometers, Detectors and Associated Equipment 521 (2004) 512–529.

[14] U. Amaldi, Cancer therapy with particle accelerators, Nuclear Physics A 654 (1999) C375–C399.

[15] T. Cybulski, O. Karamyshev, C. P. Welsch, A. Kacperek, B. Marsland, I. Taylor, A. Wray, A. Degiovanni, BEAM EMITTANCE MEASUREMENTS AND BEAM TRANSPORT OPTIMISATION AT THE CLATTERBRIDGE CANCER CENTRE, in: Proceedings of IPAC2013, Shanghai, China, 2013, pp. 810–812.

[16] T. Cybulski, A Non-Invasive Beam Current Monitor for a Medical Accelerator, Ph.D. thesis, University of Liverpool, 2017.

[17] D. E. Bonnett, A. Kacperek, M. A. Sheen, R. Goodall, T. E. Saxton, The 62 MeV proton beam for the treatment of ocular melanoma at Clatterbridge, The British Journal of Radiology 66 (1993) 907–914.

[18] UCL, Clatterbrige Proton Treatment Centre Image Maps. URL: http://www.hep.ucl.ac.uk/pbt/wikiData/clatterbridge/ImageMaps/index.html, [accessed: 01/06/2019].

[19] D. E. Bonnett, A. Kacperek, M. A. Sheen, Characteristics of a 62 MeV proton therapy beam, in: Proc. EPAC1990, 1990, p. 1787.

[20] K. Wittenburg, Halo and Bunch Purity Monitoring, CERN Accelerator School, Report No. CERN-2009-005 (2009) 557.

[21] CERN, MAD - Methodical Accelerator Design. URL: http://madx.web.cern.ch/madx/, [accessed: 01/01/2017].

[22] L. Nevay, J. Snuverink, A. Abramov, L. Deacon, H. Garcia-Morales, S. Gibson, R. Kwee-Hinzmann, H. Pikhartova, W. Shields, S. Walker, S. Boogert, BDSIM: An Accelerator Tracking Code with Particle-Matter Interactions, Computer Physics Communications (2020) 107200.

[23] S. Agostinelli, J. Allison, K. Amako, J. Apostolakis, H. Araujo, P. Arce, M. Asai, D. Axen, S. Banerjee, G. Barrand, F. Behner, L. Bellagamba, J. Boudreau, L. Broglia, A. Brunengo, H. Burkhardt, S. Chauvie, J. Chuma, R. Chytracek, G. Cooperman, G. Cosmo, P. Degtyarenko, A. Dell'Acqua, G. Depaola, D. Dietrich, R. Enami, A. Feliciello, C. Ferguson, H. Fesefeldt, G. Folger, F. Foppiano, A. Forti, S. Garelli, S. Giani, R. Giannitrapani, D. Gibin, J. J. Gomez Cadenas, I. Gonzalez, G. Gracia Abril, G. Greeniaus, W. Greiner, V. Grichine, A. Grossheim, S. Guatelli, P. Gumplinger, R. Hamatsu, K. Hashimoto, H. Hasui, A. Heikkinen, A. Howard, V. Ivanchenko, A. Johnson, F. W. Jones, J. Kallenbach, N. Kanaya, M. Kawabata, Y. Kawabata, M. Kawaguti, S. Kelner, P. Kent, A. Kimura, T. Kodama, R. Kokoulin, M. Kossov, H. Kurashige, E. Lamanna, T. Lampen, V. Lara, V. Lefebure, F. Lei, M. Liendl, W. Lockman, F. Longo, S. Magni, M. Maire, E. Medernach, K. Minamimoto, P. Mora de Freitas, Y. Morita, K. Murakami, M. Nagamatu, R. Nartallo, P. Nieminen, T. Nishimura, K. Ohtsubo, M. Okamura, S. O'Neale, Y. Oohata, K. Paech, J. Perl, A. Pfeiffer, M. G. Pia, F. Ranjard, A. Rybin, S. Sadilov, E. di Salvo, G. Santin, T. Sasaki, N. Savvas, Y. Sawada, S. Scherer, S. Sei, V. Sirotenko, D. Smith, N. Starkov, H. Stoecker, J. Sulkimo, M. Takahata, S. Tanaka, E. Tcherniaev, E. Safai Tehrani, M. Tropeano, P. Truscott, H. Uno,

L. Urban, P. Urban, M. Verderi, A. Walkden, W. Wander, H. Weber, J. P. Wellisch, T. Wenaus, D. C. Williams, D. Wright, T. Yamada, H. Yoshida, D. Zschiesche, GEANT4 - A simulation toolkit, Nuclear Instruments and Methods in Physics Research, Section A: Accelerators, Spectrometers, Detectors and Associated Equipment 506 (2003) 250–303.

[24] J. Allison, K. Amako, J. Apostolakis, H. Araujo, P. A. Dubois, M. Asai, G. Barrand, R. Capra, S. Chauvie, R. Chytracek, G. A. P. Cirrone, G. Cooperman, G. Cosmo, G. Cuttone, G. G. Daquino, M. Donszelmann, M. Dressel, G. Folger, F. Foppiano, J. Generowicz, V. Grichine, S. Guatelli, P. Gumplinger, A. Heikkinen, I. Hrivnacova, A. Howard, S. Incerti, V. Ivanchenko, T. Johnson, F. Jones, T. Koi, R. Kokoulin, M. Kossov, H. Kurashige, V. Lara, S. Larsson, F. Lei, F. Longo, M. Maire, A. Mantero, B. Mascialino, I. McLaren, P. M. Lorenzo, K. Minamimoto, K. Murakami, P. Nieminen, L. Pandola, S. Parlati, L. Peralta, J. Perl, A. Pfeiffer, M. G. Pia, A. Ribon, P. Rodrigues, G. Russo, S. Sadilov, G. Santin, T. Sasaki, D. Smith, N. Starkov, S. Tanaka, E. Tcherniaev, B. Tomé, A. Trindade, P. Truscott, L. Urban, M. Verderi, A. Walkden, J. P. Wellisch, D. C. Williams, D. Wright, H. Yoshida, M. Peirgentili, Geant4 developments and applications, IEEE Transactions on Nuclear Science 53 (2006) 270–278.

[25] J. Allison, K. Amako, J. Apostolakis, P. Arce, M. Asai, T. Aso, E. Bagli, A. Bagulya, S. Banerjee, G. Barrand, B. R. Beck, A. G. Bogdanov, D. Brandt, J. M. Brown, H. Burkhardt, P. Canal, D. Cano-Ott, S. Chauvie, K. Cho, G. A. Cirrone, G. Cooperman, M. A. Cortés-Giraldo, G. Cosmo, G. Cuttone, G. Depaola, L. Desorgher, X. Dong, A. Dotti, V. D. Elvira, G. Folger, Z. Francis, A. Galoyan, L. Garnier, M. Gayer, K. L. Genser, V. M. Grichine, S. Guatelli, P. Guèye, P. Gumplinger, A. S. Howard, I. Hřivnáčová, S. Hwang, S. Incerti, A. Ivanchenko, V. N. Ivanchenko, F. W. Jones, S. Y. Jun, P. Kaitaniemi, N. Karakatsanis, M. Karamitrosi, M. Kelsey, A. Kimura, T. Koi, H. Kurashige, A. Lechner, S. B. Lee, F. Longo, M. Maire, D. Mancusi, A. Mantero, E. Mendoza, B. Morgan, K. Murakami, T. Nikitina, L. Pandola, P. Paprocki, J. Perl, I. Petrović, M. G. Pia, W. Pokorski, J. M. Quesada, M. Raine, M. A. Reis, A. Ribon, A. Ristić Fira, F. Romano, G. Russo, G. Santin, T. Sasaki, D. Sawkey, J. I. Shin, I. I. Strakovsky, A. Taborda, S. Tanaka,

B. Tomé, T. Toshito, H. N. Tran, P. R. Truscott, L. Urban, V. Uzhinsky, J. M. Verbeke, M. Verderi, B. L. Wendt, H. Wenzel, D. H. Wright, D. M. Wright, T. Yamashita, J. Yarba, H. Yoshida, Recent developments in GEANT4, Nuclear Instruments and Methods in Physics Research, Section A: Accelerators, Spectrometers, Detectors and Associated Equipment 835 (2016) 186–225.

[26] A. inc. gafchromic^{TM} radiology, EBT3 film. URL: http://www.gafchromic.com/, [accessed: 01/01/18].

[27] S. Giordanengo, H. Palmans, Dose detectors, sensors, and their applications, Medical Physics 45 (2018) e1051–e1072.

[28] UCL, Clatterbridge Simulation Model. URL: http://www.hep.ucl.ac.uk/pbt/wiki/Clatterbridge, [accessed: 01/07/2017].

[29] J. Perl, J. Shin, J. Schümann, B. Faddegon, H. Paganetti, TOPAS: An innovative proton Monte Carlo platform for research and clinical applications, Medical Physics 39 (2012) 6818–6837.

[30] P. Chaudhary, T. I. Marshall, F. J. Currell, A. Kacperek, G. Schettino, K. M. Prise, Variations in the Processing of DNA Double-Strand Breaks Along 60-MeV Therapeutic Proton Beams, International Journal of Radiation Oncology Biology Physics 95 (2016) 86–94.

[31] J. S. L. Yap, J. Resta-Lopez, R. Schnuerer, C. P. Welsch, N. J. S. Bal, M. Fransen, F. Linde, J. L. Parsons, A. Kacperek, BEAM CHARACTERISATION USING MEDIPIX3 AND EBT3 FILM AT THE CLATTERBRIDGE PROTON THERAPY BEAMLINE, in: Proceedings of IPAC2019, 2019, pp. 8–11.

[32] M. Fuss, E. Sturtewagen, C. De Wagter, D. Georg, Dosimetric characterization of GafChromic EBT film and its implication on film dosimetry quality assurance, Physics in Medicine and Biology 52 (2007) 4211–4225.

[33] J. Sorriaux, A. Kacperek, S. Rossomme, J. A. Lee, D. Bertrand, S. Vynckier, E. Sterpin, Evaluation of Gafchromic EBT3 films characteristics in therapy photon, electron and proton beams, Physica Medica 29 (2013) 599–606.

[34] R. Dölling, Profile, Current, and Halo Monitors of the PROSCAN Beam Lines, in: Beam Instrumentation Workshop, volume 732, AIP Conference Proceedings, Knoxville, 2004, pp. 244–252.

[35] R. Dölling, S. Lin, P.-A. Duperrex, G. Gamma, B. Keil, Beam diagnostics for the proton therapy facility proscan, in: Proceedings of Accelerator Applications 2007, 2007, pp. 152–159.

[36] P. Forck, Lecture notes on beam instrumentation and diagnostics: Joint University Accelerator School, 2011.

[37] S. H. Park, S. H. Lee, Y. S. Kim, Emittance Measurement for Beamline Extension at the PET Cyclotron, Science and Technology of Nuclear Installations 2016 (2016) 1–4.

[38] K. T. McDonald, D. P. Russell, Methods of emittance measurement, in: 3rd Joint US-CERN School on Particle Accelerators: Frontiers of Particle Beams, Observation, Diagnosis and Correction, volume 343, Capri, 1988.

[39] K. Nesteruk, M. Auger, S. Braccini, T. Carzaniga, A. Ereditato, P. Scampoli, A system for online beam emittance measurements and proton beam characterization, Journal of Instrumentation 13 (2018).